A Measurement of the ^{12}C(n, 2n) Cross Section from Threshold to 26.5 MeV

Thomas Eckert, August Gula, and Mark Yuly. Houghton College.

Overview and Results

A measurement of the ^{12}C(n, 2n) cross section from threshold to 26.5 MeV was made using the 4.5 MV tandem van de Graaff accelerator at Ohio University (OU). These cross sections are needed to use this reaction as a diagnostic tool for characterizing inertial confinement fusion (ICF) implosions at the National Ignition Facility (NIF) once ignition is reached. As seen in Figure 1, there is disagreement between reported values from previous measurements [1-7], motivating this new experiment.

A feasibility test in 2012 was followed by a 10 day data collection run at Ohio University during the summer of 2013. The OU experiment yielded two of the three values needed to compute the cross section at each neutron energy, specifically, the number of detected ^{11}C decays and the incident neutron flux. The last value needed is the absolute detector efficiency, which allows the detected number of ^{11}C decays to be converted into the absolute number of ^{11}C nuclei formed. A simulation was written using the GEANT framework, then used to calculate both the coincidence and singles efficiencies. These were then used to compute the measured cross sections for both the graphite and polyethylene target. The preliminary results are shown in Figure 1. The rms percent difference between the measured cross section using each of the six target and detector combinations and the average for all the methods, for a given energy above threshold, is typically around 4% to 5%, and the average percent difference for all the energies is about 7%. However, the coincidence efficiency in graphite is systematically high. Removing these values yields an rms for the remaining configurations of only 4%. Validating the normalization of the efficiencies predicted by the GEANT simulation has been the focus of our work the past two summers.

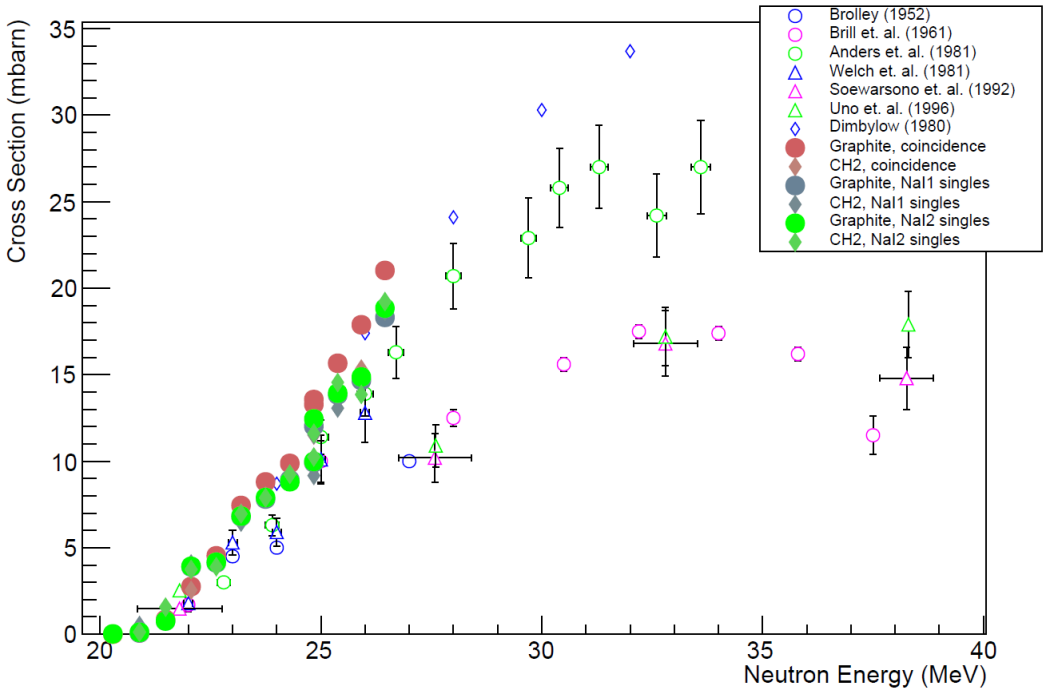

Figure 1. Preliminary cross sections for the ^{12}C(n,2n)^{11}C reaction (solid symbols) determined using the coincidence (green) and singles from detector 1 (red) and detector 2 (blue) with the graphite (circles) and polyethylene (diamonds) targets Previous measurements (open symbols) are from Brolley et al. [1] (blue circles), Brill et al. [2] (pink circles), Anders et al. [3] (green circles), Welch et al. [4] (blue triangles), Soewarsono et al. [5] (pink triangles), Uno et al. [6] (green triangles), and Dimbylow [7] (blue diamonds).

Analysis of Singles and Coincidence Growth Curves

The experiment performed at OU was described in detail in the 2013 report [8] to the Laboratory for Laser Energetics (LLE), and will only be summarized here. As shown in Figure 2, deuterons from the accelerator were allowed to strike a thin tritium target, producing monoenergetic neutrons via ^{3}H(d,n)^{4}He. These neutrons could then hit two targets, a polyethylene and a graphite disk, both containing ^{12}C, and initiate the ^{12}C(n, 2n)^{11}C reaction. Neutrons striking the polyethylene target could also scatter elastically from the hydrogen nuclei present in the material. These protons could then travel through a hole in the graphite disc to be counted by a dE-E detector. By using the np elastic scattering cross section, which has been well measured [9], the neutron flux on the polyethylene target was determined. Corrections, which never exceeded about 8%, were calculated to account for the dependence of the ^{3}H(d,n)^{4}He and ^{1}H(n,p)n reactions on incident energy and angle, and for effect on solid angle of the hole in the graphite.

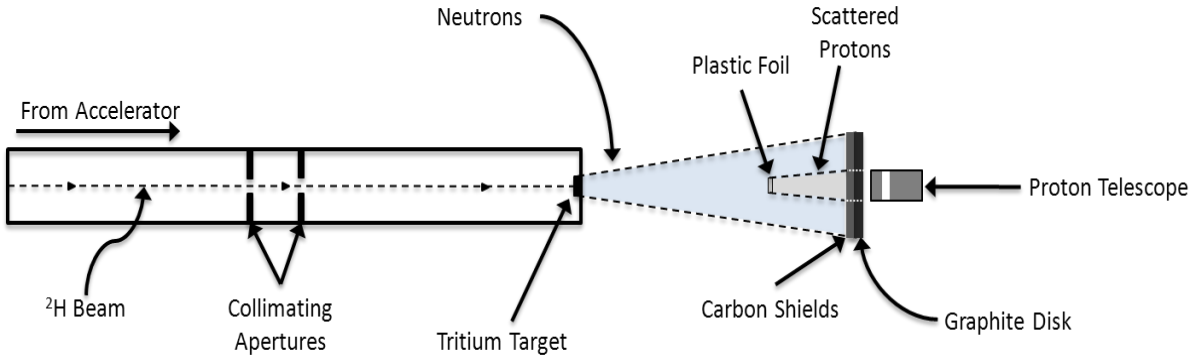

Figure 2. The 2013 Ohio University experiment. Neutrons produced by deuterons striking a tritium target are allowed to hit polyethylene and graphite targets.

The ^{11}C decays in the activated polyethylene and graphite targets were counted using pairs of 3 inch diameter by 3 inch long NaI detectors "sandwiching" each target , capable of counting the 511 keV gamma rays from positron annihilation in both singles and coincidence mode simultaneously. Pulses from all of these detectors were sent to a Fast ComTech MPA-4 system, which recorded the pulse heights and timing information. This allowed the ^{11}B growth curves from $^{11}C \rightarrow {}^{11}B + e^{+} + \nu$ to be measured for both singles and coincidence events, and fit with the exponential growth function

$$R(t) = R_0\left(1 - e^{-\lambda t}\right) + At + B \tag{1}$$

where $R(t)$ is the sum of all the positron annihilation gamma rays detected up to time *t*, R_0 is the initial ^{11}B growth rate, and $At + B$ is the integral of the constant rate of background events. The number of ^{11}C nuclei present in the sample, N_{C11}, is then

$$N_{C11} = \frac{R_0 e^{\lambda\, t_{trans}}}{\varepsilon} \tag{2}$$

where t_{trans} is the time between the end of activation and the start of counting, in other words, the time required to transfer the samples to the counting station, and ε is either the absolute full-peak coincidence or singles efficiency, depending on how the growth curve was generated.

Cross sections for ^{12}C(n, 2n) were extracted using N_{C11}, the number of elastically scattered protons detected, N_P, and the activation time, *t*, since

$$\sigma = \frac{N_{C11}}{T_C}\,\frac{\lambda}{1 - e^{-\lambda t}}\left(\frac{N_P}{N_n}\right)\frac{1}{N_P} \tag{3}$$

where λ is the decay constant for ^{11}C, and T_C is the target thickness in terms of carbon nuclei (carbon nuclei/cm^2). The fraction N_p/N_n is the number of protons detected, N_p, for a given number of neutrons, N_n, striking the polyethylene

target. This quantity was calculated for the experiment geometry using the known $^{3}H(d,n)^{4}He$ [10] and np elastic scattering [9] cross sections.

Several new analysis tasks were carried out this summer:

1. Singles Events

In addition to the coincident data, new growth curves were also generated using singles events from each NaI detector individually, fit using Eq. (3) , and used to calculate cross sections using Eq. (3). Figure 3 shows a typical ADC energy spectrum from detector 1 with an activated graphite disk between NaI detector 1 and 2, collected for about 2 hours. The difference between the spectrum in coincidence with detector 2 (left) and the singles spectrum (right) is dramatic – the 511 keV peak is barely visible in the singles spectrum. For the polyethylene target, which is much thinner than the graphite, the 511 keV peak is not visible because there are only about 7000 ^{11}C decays over a 2 hour period – a very small number in comparison to the background.

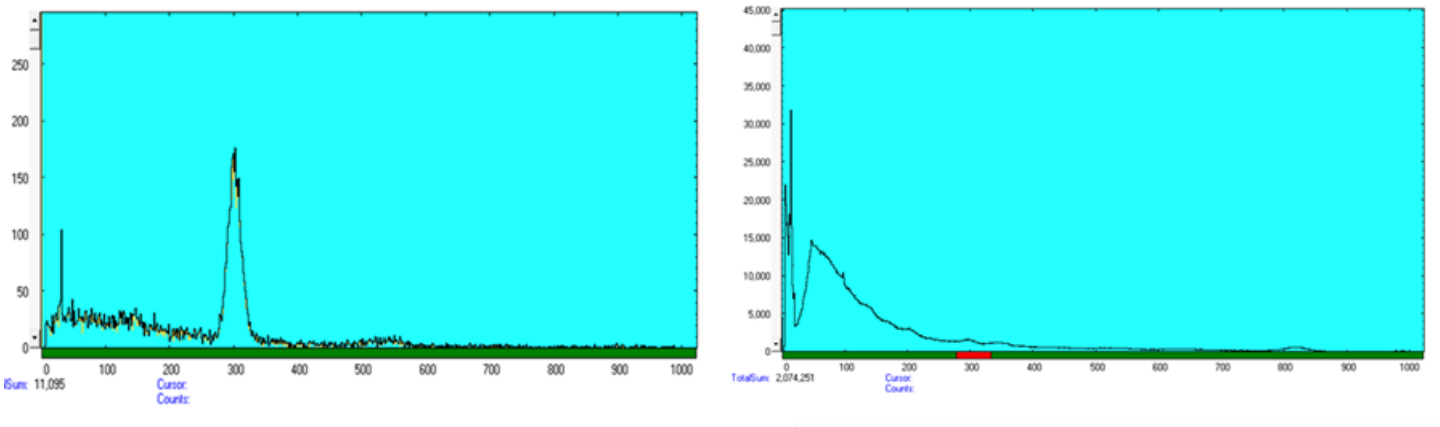

Figure 3. The energy spectra for NaI detector 1, for singles events (right) and for events in coincidence with a 511 keV gamma ray striking NaI detector 2 (left). The histograms plot the number of events as a function of energy deposited in the detector, in channels. The red region of interest in the singles spectrum indicates the location of the 511 keV peak. The advantage of the coincidence technique is clear.

Figure 4 shows a typical fit of Eq. (1) to the coincidence and singles growth curves. These growth curves were created by integrating the number of events in the 511 keV peak up to time t, and plotting the integral as a function of t. The exponential nature of the growth curve is clear for coincidence events, but because of the large number of background events relative to the number of ^{11}C decays, the singles growth curve for the thin polyethylene targets is nearly a straight line. Nevertheless, the value of R_0 can still be extracted from these fits and used to determine the cross section using Eq. (2), albeit with a larger uncertainty.

The cross sections generated using the singles data are plotted along with the coincidence results in Figure 1, with good agreement between the two different targets, with different geometries and materials, as determined using singles events from each detector individually and both detectors in coincidence.

2. Distribution of ^{11}C within the Graphite Disk

Because of the geometry of the neutron source and detector, as well as neutron reactions that can occur in the graphite (the mean free path is about 6 cm, making the graphite thickness about 15% of the MFP) the $^{12}C(n, 2n)$ reactions will be distributed non-uniformly throughout the target. Because it is so thin, this effect is not significant for the polyethylene disk.

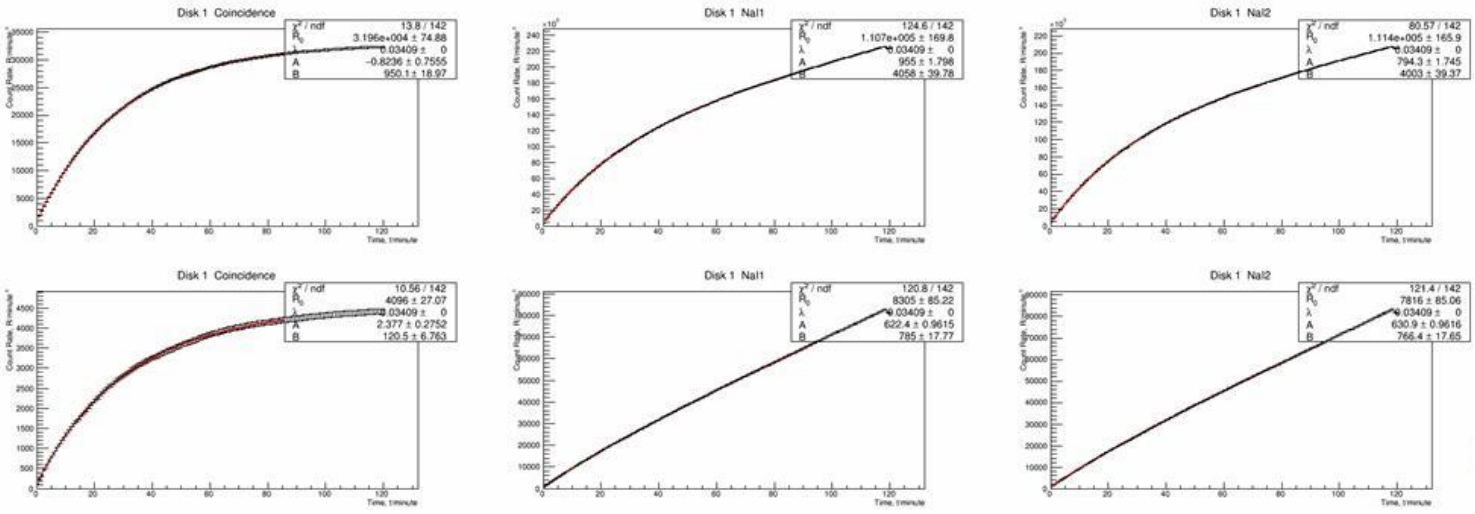

Figure 4. Fits of Eq. (1) to the growth curves for the graphite (top row) and polyethylene (bottom row) targets activated by 26 MeV neutrons. The histograms show the integrated number of events as a function of the time in minutes. The exponential component of the growth curve is clearly seen in the coincidence curves (leftmost column) while the singles from detector 1 (center column) and detector 2 (right column) are more linear due to the large background, especially for the thin polyethylene targets.

The Monte Carlo simulation code MCNP5 was used to calculate the distribution of ^{11}C nuclei in the graphite disk. In the simulation, monoenergetic neutrons were emitted uniformly and isotropically from a circular region on the flat tritium target, with a radius equal to that of the last upstream collimator on the deuteron beam. The number of $^{12}C(n, 2n)$ reactions at the front and back faces of a graphite disk were measured for the geometry of the experiment. The standard MCNP cross section library for $^{12}C(n,2n)$, which is based on past data [1-7], was used. The front to back ratio of the $^{12}C(n,2n)$ rate is shown in Figure 5 as a function of neutron energy. It varies about one percent from the center to the edge of the graphite disk, and a couple of percent across the energy range of interest. The neutron energy stayed approximately monoenergetic, at least to the 0.1 MeV level of interest.

Simulating this effect in with GEANT changes the absolute full-peak singles efficiency by about 3%, raising it 3% on the high side and reducing it 3% on the low side. For coincidences this lowers the full-peak efficiency by about 2%. Unfortunately the orientation of the graphite targets between the NaI detectors was never recorded and so this effect cannot be easily corrected in the cross sections, and are not accounted for in Figure 1.

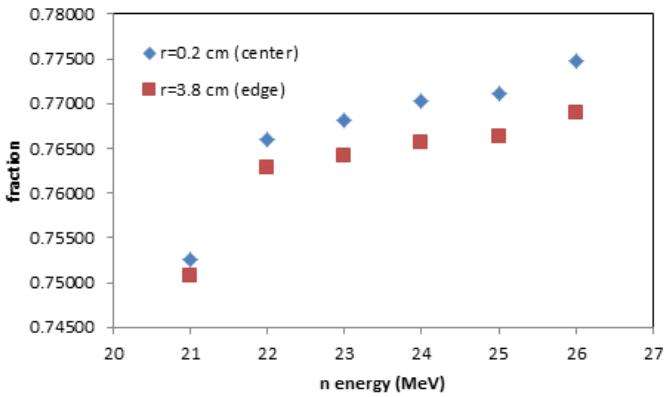

Figure 5. The ratio of the number of ^{11}C produced to the front face to the number produced at the back face of the graphite disk by the $^{12}C(n, 2n)$ reaction as a function of incident neutron energy, calculated using the MCNP5 simulation. The ratio varies by about one percent from the center (blue diamonds) to the edge (red squares) of the disk, and by a couple of percent across the energy range of interest.

Calculating the Absolute Full-peak Efficiencies for Singles and Coincidence

In order to accurately measure the $^{12}C(n, 2n)$ cross section, after 2013 the only remaining unknown quantity was the absolute full-peak detector efficiency, ε in Eq. (2). Starting in September of 2013, and continuing through the summer of 2014, a series of experiments were performed to measure this efficiency for both singles and coincidence events. In these initial experiments, which are described in detail in the 2014 report [11] to LLE, a novel associated particle technique was used to allow the efficiencies to be determined using an uncalibrated positron source. In this technique, another detector, either a silicon surface barrier detector or a plastic scintillator, was used to stop the positrons from a ^{22}Na source. The fraction of events from the silicon or plastic detector for which the NaI detector was also triggered in coincidence is the absolute efficiency.

One difficulty with using ^{22}Na as the positron source is that most of the time a 1.274 MeV gamma ray is released along with the positron. These gamma rays sum with the 511 keV positron annihilation gamma rays in the detector, and this artificially reduces the full-peak efficiency. To correct for this, another NaI detector was placed nearby, and the requirement was added that this detector also detect a full-peak 1.274 keV gamma ray. If the 1.274 keV gamma ray hits this additional detector, then it did not enter the NaI detector we are measuring the efficiency of, and so summing events are eliminated.

For the $^{12}C(n, 2n)$ analysis, however, the efficiencies needed are for a 7.62 cm diameter graphite disk, sandwiched between the two detectors which are separated by only 0.89 cm, and for a 2.54 cm diameter polyethylene disk, centered between the detectors with separation 1.64 mm. In these disks, ^{11}C is distributed, approximately uniformly in the polyethylene, and according to Figure 5 for the graphite. Clearly, there is no way that a source can be devised to allow the efficiencies to be measured for these geometries and source distributions. The solution to this problem was to develop a Monte Carlo simulation code, using the Geant4 toolkit [12], to simulate the interactions of the gamma rays, electrons and positrons in the detectors and source to predict the efficiencies.

Because of the extreme sensitivity of the efficiency to the dimensions and materials of the source and detectors, we planned to use the efficiency measurements to validate our GEANT simulations. The GEANT code would then be used to determine the efficiencies for the actual geometries used in the $^{12}C(n, 2n)$ experiment.

Unfortunately, at the end of 2014 the agreement between the calculated and measured efficiencies was still poor – and it was not clear whether the problem was the experiment or the calculation. Because of this we obtained calibrated ^{22}Na and ^{68}Ge sources from Ryan Fitzgerald in the Radiation Physics Division of the Radioactivity Group at the National Institute of Standards and Technology (NIST) and devised a new experiment which we carried out this past summer.

Experiment Design

The concept behind the experiment is illustrated in Figure 6. For the initial measurement, approximately 0.1 μCi NIST calibrated Eckert and Ziegler ^{68}Ge source, with activity measured to $\pm 1.7\%$, was sandwiched between 1.59 mm thick copper disks of 2.49 cm and 2.39 cm diameter. The source had a 3 mm active diameter deposited in the center on the face of a 25.4 mm diameter aluminized Mylar disk of thickness 0.254 mm. The active side was covered with a 0.071 mm thick layer of Kapton. The source assembly was then placed between the two 7.62 cm diameter by 7.62 cm long cylindrical NaI detectors, with a set distance from the active ^{68}Ge deposit and the front face of each detector. The detectors and source were mounted using sliding positioners approximately 20 cm above an optics rail.

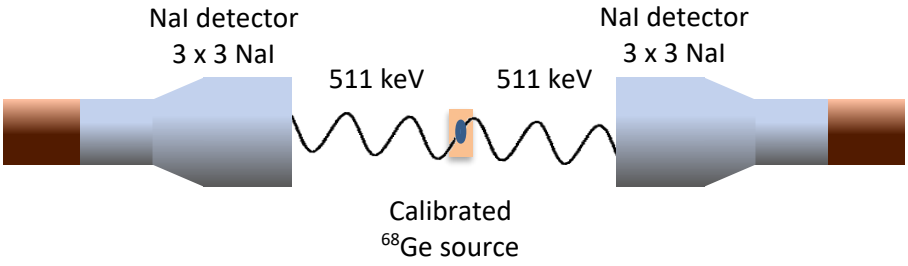

Figure 6. Conceptual schematic for the coincidence efficiency experiment. Positrons from a calibrated ^{68}Ge source annihilate in graphite or copper disks that are placed on with side of the thin source. The resulting annihilation gamma rays are detected by two collinear NaI detectors.

The ^{68}Ge source is particularly advantageous for this measurement, since its emission of high energy gamma rays is very weak. Figure 7 shows the decay chain for ^{68}Ge. This isotope decays entirely by electron capture to ^{68}Ga, emitting only low energy x-rays and Auger electrons. The ^{68}Ga decays by positron emission (87.85%) and electron capture (8.92%) to the ground state ^{68}Zn, or by positron emission (1.29%) and electron capture (1.93%) to the first excited (1077 keV) state of ^{68}Zn. Thus the overall branching ratio for positron emission is 89.14%. The endpoint energy for decay to the ground state is 1899 keV, which give the positrons a considerable range; even in copper they can travel up to about 1.59 mm, which is how the thickness of the copper disks was chosen.

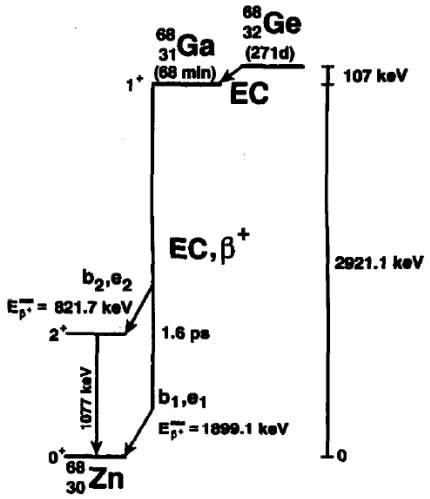

Figure 7. Decay chain for ^{68}Ge, which decays to ^{68}Ga with half-life 270.95 days, which then decays into ^{68}Zn with half-life 67.71 min. Very few high energy gamma rays result. Figure from Ref. [13].

The detectors were aligned using a theodolite approximately 5 m from the detectors, along the axis of the detectors. This allowed the center axes of the detectors and source to be made collinear to approximately ± 1 mm. Along the axis, the distance between the front face of each detector and the active region of the source was with an accuracy of approximately ± 0.5 mm using a CCD camera.

Figure 9 shows the electronics diagram for the experiment. Signals from each detector were amplified and a logic timing pulse produced for each by the timing single channel analyzer (TSCA) modules. The data acquisition event trigger was a logic pulse from either of the two detectors, whichever came first. This trigger allowed either detector or both in coincidence to cause the event to be recorded, thereby allowing both singles and coincidence data to be acquired simultaneously. The singles and coincidence events were later be sorted out by the analysis code, using either the time difference between the detectors or the hardware coincidence. A hardware coincidence between the two detectors was also formed, for the purpose of checking the live times and also as a way to test coincidence conditions formed in software using the timing information from the TDC.

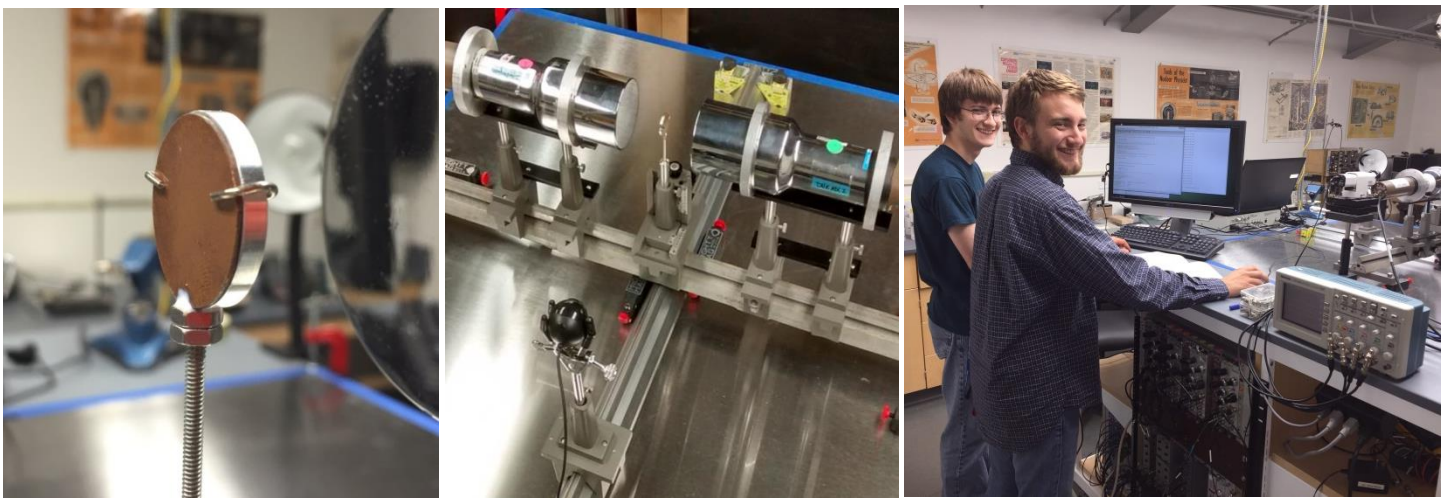

Figure 8. The ^{68}Ge source assembly (left) and the source assembly placed between the two NaI detectors (center). The camera is used for precisely positioning the detectors relative to the active region on the source. NIM and CAMAC electronics process and digitize the detector pulses which are read out into the computer (right).

The logic pulses from the TSCA for each detector were used to stop a LeCroy 3377 time-to-digital converter (TDC), which was started by the event trigger, allowing the time difference between the detectors to be calculated regardless of which signal came first. The FWHM of the time difference coincidence peak is approximately 60 ns.

The timing pulses from the detectors were also used to form the gate for the ORTEC 413AD analog-to-digital converter (ADC), which digitized the pulse heights from each of the detectors. Following an event trigger pulse, a gate generator was used to deactivate the circuit for approximately 20 μs to allow time for the ADC conversion. A LeCroy 2551 scaler was used to record the number of pulses generated by each detector for the purpose of calculating the live time. The live time fraction was typically only about 25%.

The CAMAC modules were read out using the SCSI interface of a Jorway 73A CAMAC crate controller into a PC microcomputer running Linux. A custom C++ data acquisition code was written using the SJY CAMAC drivers [14] from Fermilab and the ROOT data analyses framework [15]. The data were analyzed using a set of custom ROOT macros.

Figure 10 shows a typical time spectrum for TDC 0, which always stops on pulses from detector NaI1, but can start on NaI1 or NaI2. There are several possible sequences of events. If NaI1 is the first detector to trigger, then NaI1 starts the TDC, and these events will fall in the "self-timing peak" shown in Figure 10. On the other hand, if NaI2 triggers first, the event will be recorded with the time difference between NaI2 and NaI1. Of course, if there is no signal from NaI1, the timer can still start on a pulse from NaI2, but it will never stop, and these events are recorded as a time difference of -1.

Typical energy spectra for singles and coincidence events are shown in Figure 11. By selecting events that are in the 511 keV peak in the singles spectra, the absolute full-peak singles efficiency can be found using

$$\varepsilon(\text{singles}) = \frac{\text{NaI1/live fraction}}{^{68}\text{Ge decays} \cdot \text{branching ratio} \cdot 2} \tag{4}$$

where the factor of two accounts for the fact that there are two gamma rays emitted for each ^{68}Ge decay, and the coincidence efficiency

$$\varepsilon(\text{coincidence}) = \frac{(\text{NaI1} \cdot \text{NaI2})/\text{live fraction}}{^{68}\text{Ge decays} \cdot \text{branching ratio}} \tag{5}$$

is formed by counting the number of events with both detectors registering pulses inside the 511 keV peak.

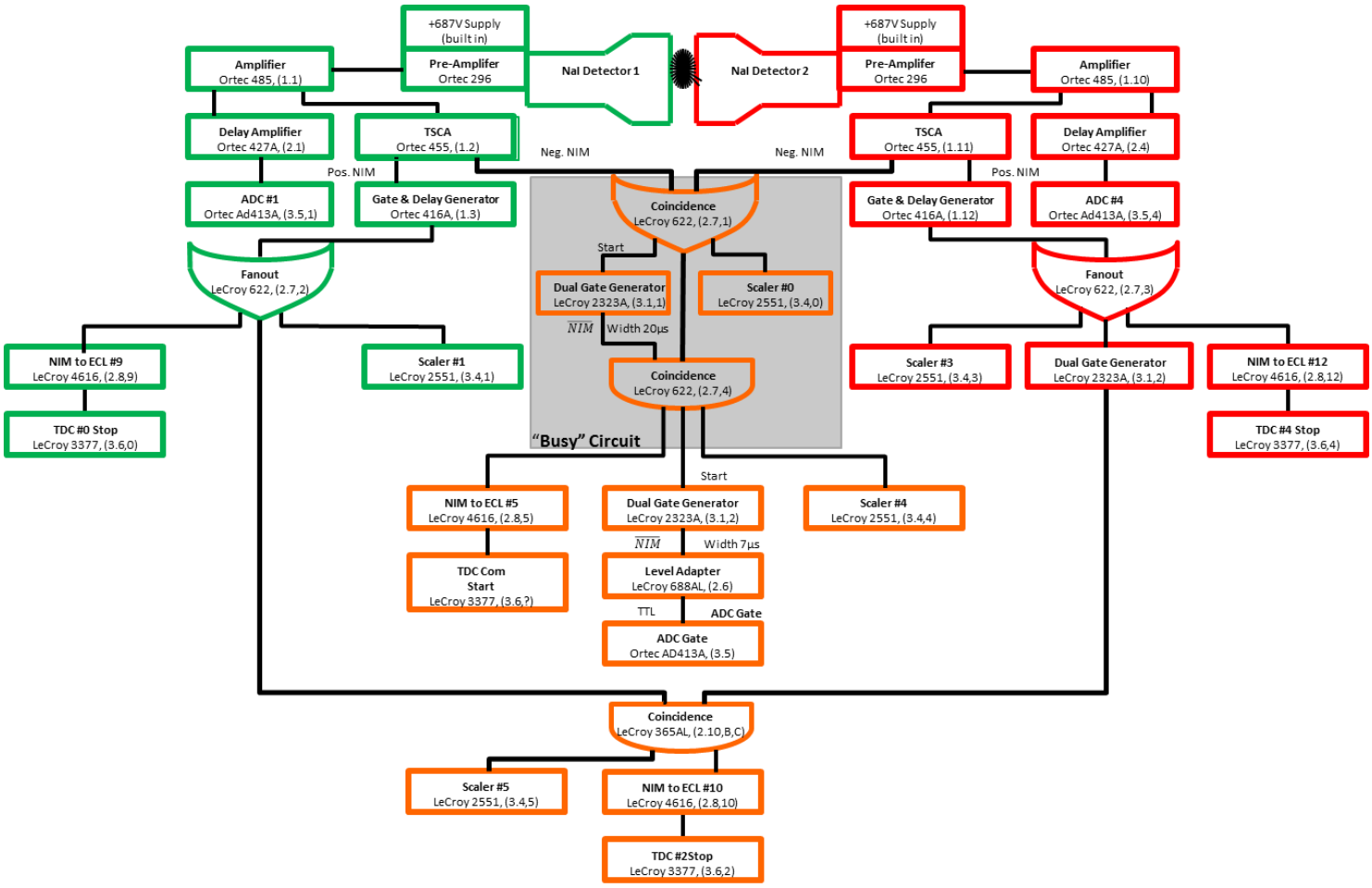

Figure 9. Electronics diagram for the CAMAC system used to digitize time differences and pulse heights from the detectors.

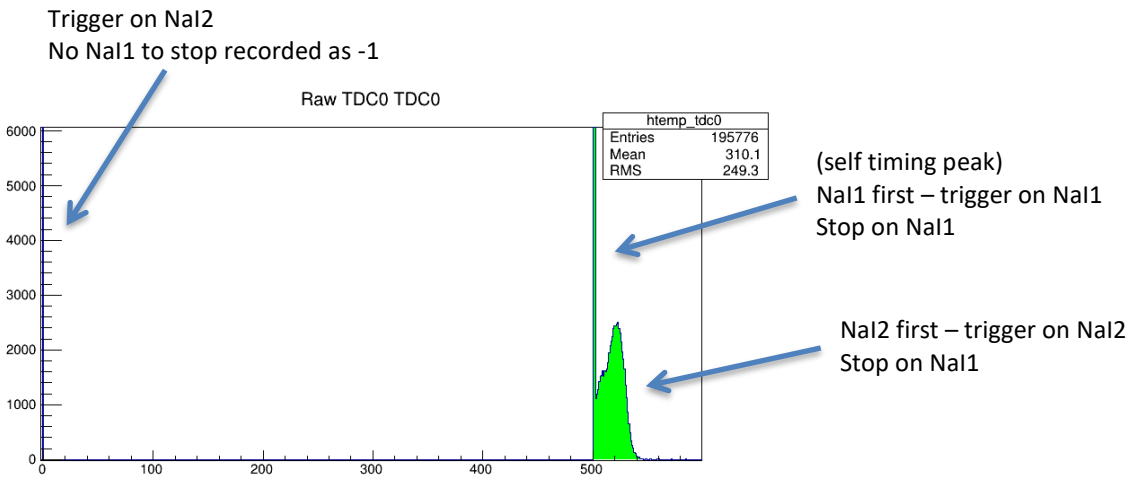

Figure 10. Histogram of the timing spectrum for the NaI1 detector. This TDC always stops on NaI1, but can start on either the NaI1 or NaI2 detector.

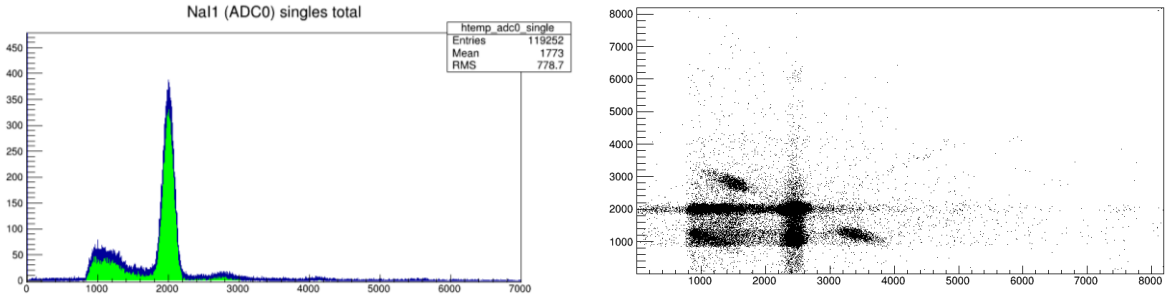

Figure 11. Histograms of the energy spectrum for singles events in detector NaI1 (left) and coincidence events (right). These were used to determine the number of events in the 511 keV peak both for a single detector and in coincidence.

GEANT Simulation

A GEANT simulation of the experiment was also created. In this simulation code, 100,000 ^{68}Ga decay events are generated randomly in the ^{68}Ge source. For events which decay by positron emission, the simulated positrons are emitted isotopically with energies according to the positron decay energy spectrum for ^{68}Ga. These positrons are tracked through the various materials present in the source and the copper disks, until they annihilate with an atomic electron. The resulting gamma rays are then tracked as they exit the source and travel through the air. Some of them enter the detectors and can interact, depositing energy in the NaI crystals. This can be used to generate a simulated energy spectrum, such as the example shown in Figure 12. The events with energies below 511 keV are due to Compton scattering, mostly from one detector into the other. The abrupt cut off in the measured spectrum below 250 keV results from the threshold setting for the single channel analyzer. The peak at 700 keV is most likely summing between the Compton scattered gamma rays and 511 keV annihilation gamma rays. The 1077 keV peak from the decay of the first excited state of ^{68}Zn is small but present, as is the peak resulting from summing with the 511 keV gamma rays. The GEANT simulation 511 keV peak appears larger than the measured peak, but the areas are nearly the same – the measured peak is just slightly wider. The measured intensity for energies larger than the 511 keV peak appear larger than the calculated values, but this is because of room background, which is not included in the simulation.

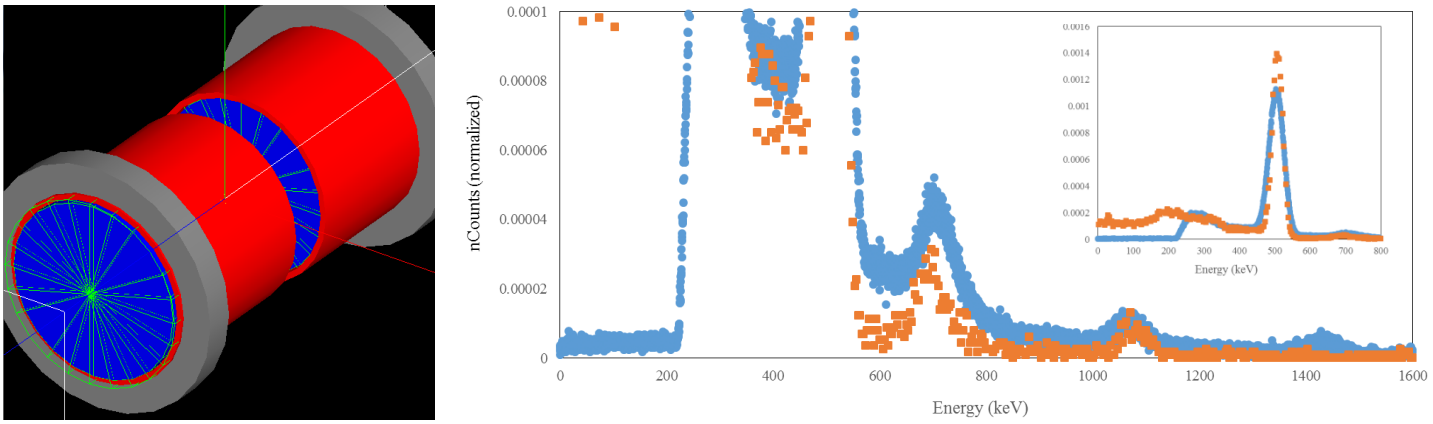

Figure 12. Geometry of the experiment used by the GEANT simulation (left) and the results of the experiment and GEANT simulation (right) showing the simulated (orange) and measured (blue) energy spectra. The inset has a scale on the y axis that allows the 511 keV peak to be examined.

These GEANT generated energy spectra were also analyzed using Eq. (4) and (5) to get the predicted absolute full peak efficiency. The predictions were then compared with the measured efficiencies as a test of the GEANT code and found to overpredict the efficiency. At large distances (greater than about 8 cm) the singles efficiency prediction agreed with the measured efficiencies, but as the distance between the source and detector was decreased the disagreement increased -- at 0.65 cm the GEANT simulation overpredicted by about 20%. For coincidence efficiencies, the simulation overpredicted the efficiency by about 12% at large distances, and 30% at 0.65 cm.

It is believed that the cause of this discrepancy is the presence of a reflecting layer surrounding the NaI crystals in the detector. Experience with other similar NaI detectors has found reflecting layers between 2 mm and 5 mm thick, composed of various reflective materials such as BaO powder, Al_2O_3 powder, and Teflon tape with densities of approximately 0.9 to 5 g/ml. This layer is not described in the detector data sheets, and so the manufacturer has been contacted and plans have been made to x-ray one of the detectors. In the GEANT predictions that follow, a reflecting layer 2.7 mm thick and composed of BaO has been assumed. This assumption was made because it gave good agreement with the full-peak efficiencies that were measured using graphite disks, described later.

Comparison of GEANT predictions with Summer 2014 measurements

Before comparing the results of the GEANT calculation to measurements made this summer with the calibrated sources, it is worthwhile to go back and reexamine the efficiency data collected last summer using the beta coincidence technique (see Ref. 11 for a complete description). In the GEANT simulation of this experiment, several simplifying assumptions were made. First, the plastic scintillator, which was a 9.5 mm square made from 5.4 mm thick BC-400 plastic scintillator with wells milled on each side leaving a 2 mm thick membrane between the two sides, was simulated as a circle of radius 4.75 mm with the other dimensions remaining the same. Since in this experiment a NaI detector was used to make certain that no 1.274 MeV gamma rays from the ^{22}Na source hit the other detectors, the source in the simulation was made to simply emit positrons in random directions into the plastic scintillator, with an energy distribution that approximated that of ^{22}Na.

The results of this simulation are shown in Figure 13, along with the measured absolute full-peak singles and coincidence efficiencies, as a function of the spacing between the source and the detectors. Even with the simulation approximations described, the agreement is quite good with the detectors moved back 2.7 mm to allow space for a reflector.

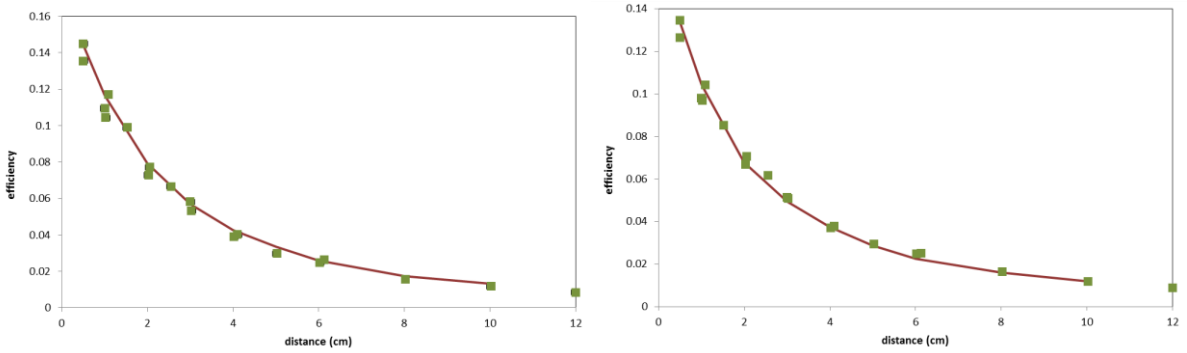

Figure 13. Plot of singles NaI1 (left) and coincidence (right) absolute full-peak efficiency measured (green squares) using beta coincidence technique (Summer 2014) and predicted (red curves) by the GEANT simulation.

Efficiency Results for Copper Disks

The results of a series of measurements made by placing the calibrated ^{68}Ge source at different distances from the two detectors, with the source sandwiched between the two copper disks as described earlier, are shown in Figure 14 for singles and Figure 15 for coincidence efficiency. Here the agreement with the GEANT model, while still much better than without the 2.7 mm thick reflector, is less good. For singles, at short distances the model does well, but as the separation between the source and detector grows so does the disagreement, eventually reaching about 15% at 10 cm. For coincidences, the model seems to be approximately constant but 5% low. This discrepancy could simply be the result of the assumed thickness and composition of the unknown reflector – in fact, a recalculation of the efficiency with a 2.5 mm thick reflector is much better. Alternatively, it could result from the 0.25 mm thick decal of unknown composition that was attached to the source while these measurements were made. The efficiency is very sensitive to

the details of the immediate environment around the source, and it is possible that even this small change could lead to a 5-15% effect.

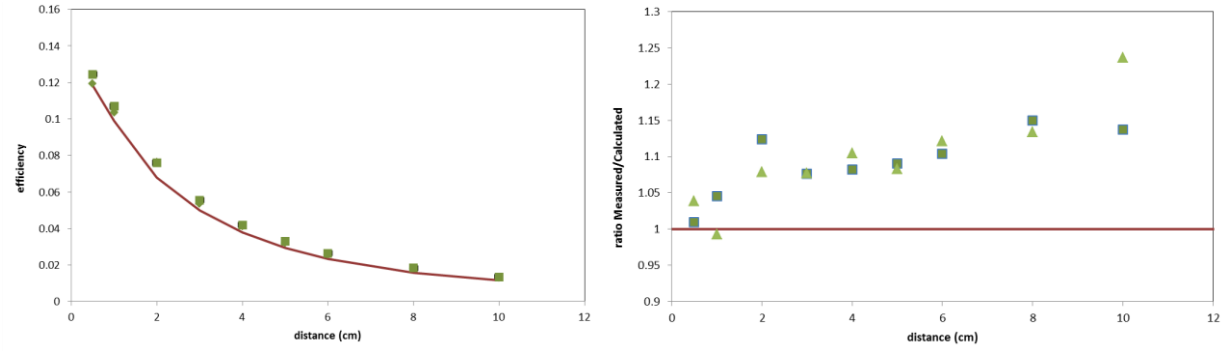

Figure 14. (Left) Plot of predicted singles absolute full-peak efficiency (red curve) as a function of distance between the source and detectors, for NaI1 (green diamonds) and for NaI1 but with the source rotated 180° (green squares) to check for systematic problems due to asymmetry. (Right) Plot of the ratio of the measured to GEANT-calculated full-peak efficiencies for singles events for NaI1 (green squares) and NaI2 (green diamonds). Agreement between prediction and measurement would yield a value of 1.0 (red line). These measurements were made with the source sandwiched between the copper disks.

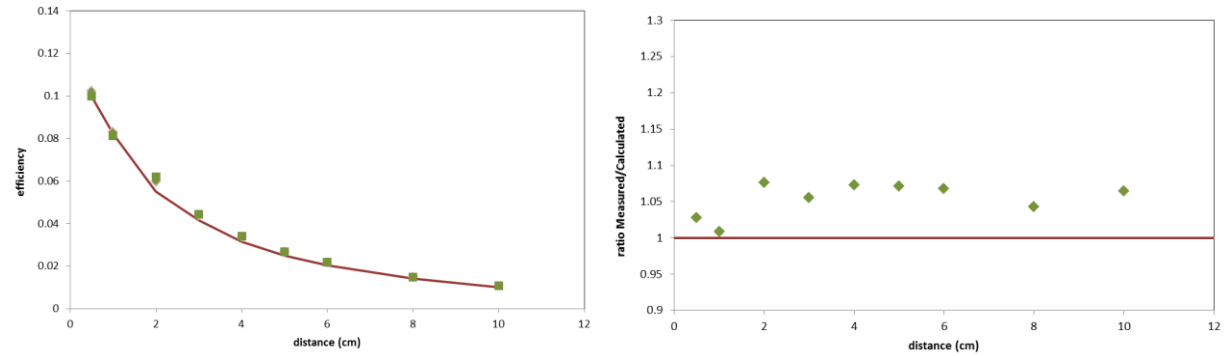

Figure 15. (Left) Plot of predicted (red curve) and measured (green squares) coincidence absolute full-peak efficiency as a function of distance between the source and detectors. (Right) Plot of the ratio of the measured to GEANT-calculated full-peak efficiencies for coincidence events (green diamonds). Agreement between prediction and measurement would yield a value of 1.0 (red line). These measurements were made with the source sandwiched between the copper disks.

Efficiency Results for Graphite Disks

Another set of measurements, this time with the decal removed, were made with the source sandwiched between graphite disks of diameter 7.62 cm and density 1.84 g/cm^3. On each side of the source there were two disks, each 0.89 cm thick. The entire assembly, graphite disks plus source, was placed between the two NaI detectors and held in place by them. A series of measurements, shown in Figure 16, were made by moving the source radially outward from the center of the graphite disk. Here the GEANT simulation for singles agrees within a few percent all the way out to nearly the edge of the graphite. The coincidence predictions are less good, but nevertheless agree well near the center where the efficiency is highest. This test is the most like the situation in the ^{12}C(n, 2n) experiment, in which the positrons are interacting in a graphite disk of the same diameter and similar thickness, and being detected by the same NaI detectors that are pressed up directly against the graphite.

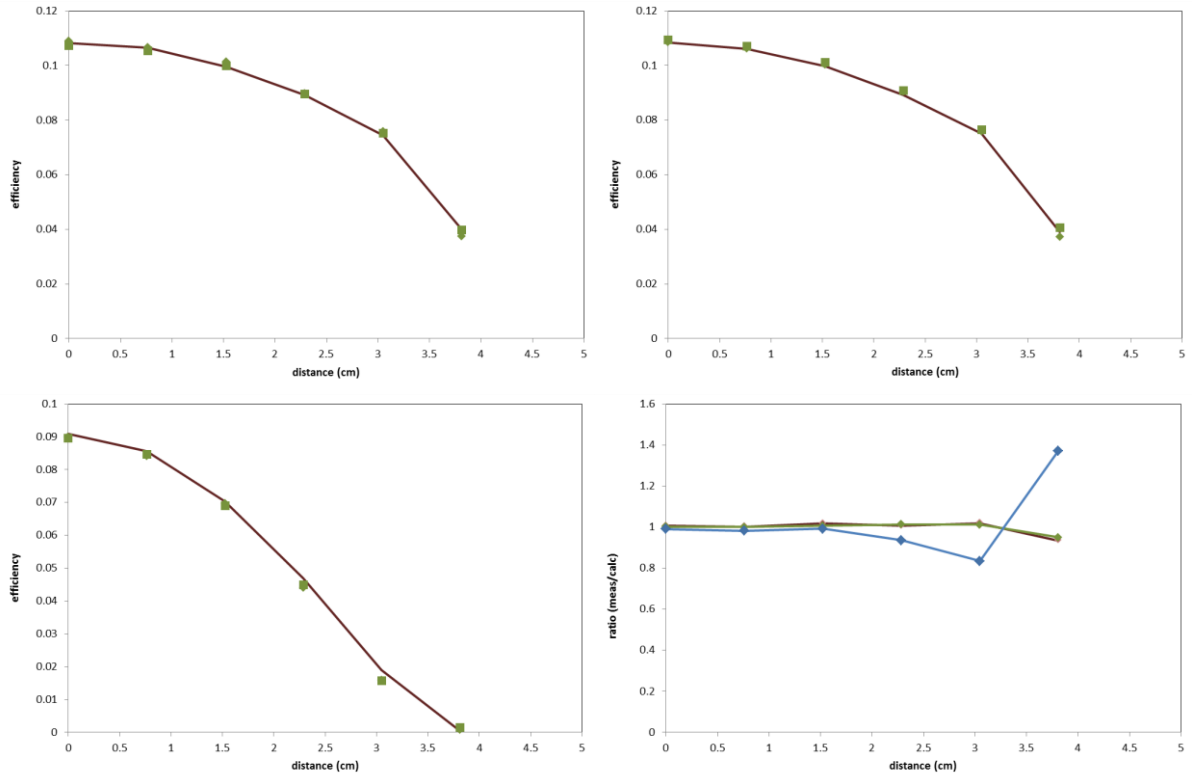

Figure 16. Plot of singles NaI1 (top left), NaI2 (top right), and coincidence (bottom left) absolute full-peak efficiency measured (green squares) and predicted (red curves) by the GEANT simulation for the ^{68}Ge source sandwiched between graphite disks. The ratio of the measured to predicted efficiencies is plotted (bottom right) for NaI1 (red), NaI2 (green) and coincidence (blue).

Conclusions

The remaining unknown required to complete the ^{12}C(n, 2n) cross section measurement are the absolute full-peak coincidence and singles efficiencies. Because it is impossible to reproduce a calibrated ^{11}C source with the distribution and shape of the targets used in the ^{12}C(n, 2n) experiment, a GEANT simulation has been created to model the source and detector system allowing the efficiencies to be calculated. In order to validate the computer model, several experiments have been performed in which the efficiencies have been measured for various source and detector configurations, and with two very different experimental techniques.

These experiments confirmed that the model can be used to predict efficiencies to better than 5%, but only with the inclusion of a small gap between the aluminum detector can and the NaI crystal of the detectors. Although it is not shown in the manufacturer specifications, most detectors surround the NaI crystal with a few millimeters of reflecting material. We are currently attempting to verify this with the manufacturer, and have made arrangements for one of the NaI detectors to be x-rayed at the NIST Physical Measurement Laboratory in Maryland.

These efficiencies have been used to calculate the preliminary cross sections shown in Figure 1. The remaining analysis tasks are to examine reasons for the systematically high cross sections from the graphite target coincidence data, and to carefully analyze the measurement uncertainties. We intend to write a paper describing our results this fall, to be submitted before the end of this academic year.

Presentations

Thomas Eckert, Laurel Vincett, Mark Yuly, Stephen Padalino, Megan Russ, Mollie Bienstock, Angela Simone, Drew Ellison, Holly Desmitt, Craig Sangster, and Sean Regan, **"Coincidence Efficiency of Sodium Iodide Detectors for Positron Annihilation,"** 56th Annual Meeting of the APS Division of Plasma Physics, New Orleans, Lousiana, October 27-31, 2014; Penn-York Undergraduate Research Association Conference, Houghton College, Houghton, NY 14744. Nov. 1, 2104; XXXIV Annual Rochester Symposium for Physics Students, SUNY Oswego, Oswege, NY, April 11, 2015; Omega Laser User's Group Meeting, Laboratory for Laser Energetics, Rochester, NY, April 22-24, 2015.

Mark Yuly, Thomas Eckert, Garrett Hartshaw, Ian Love, Keith Mann, Tyler Reynolds, Laurel Vincett, Stephen Padalino, Megan Russ, Mollie Bienstock, Angela Simone, Drew Ellison, Holly Desmitt, Carl Brune, Thomas Massey. Ohio University, Ryan Fitzgerald, Mollie Bienstock, Craig Sangster, Sean Regan, **"The 12C(n,2n)11C Cross Section from 20-27 MeV,"** Science and Technology Seminar, Laboratory for Laser Energetics, University of Rochester, Rochester, N.Y., July 18, 2014.

This material is based upon work supported by the Department of Energy [National Nuclear Security Administration] University of Rochester "National Inertial Confinement Program" under Award Number(s) DE-NA0004144.

---

[1] J. E. Brolley Jr., J. L. Fowler, and L. K. Schlacks, Phys. Rev. **88**, 618 (1952).
[2] O. D. Brill, N. A. Vlasov, S. P. Kalnin, and L. S. Sokolov, Sov. Phys. Doklady **6**, 24 (1961).
[3] B. Anders, P. Herges, and W. Scobel, Z. Phys. A **301**, 353 (1981).
[4] P. Welch, J. Johnson, G. Randers-Pehrson, and J. Rapaport, Data file EXFOR-12912.004, compare Bull. Am. Phys. Soc. **26**, 708 (1981).
[5] T. S. Soewarsono, Y. Uwamino, and T. Nakamura, JAERI Tokai Rep. **27**, 354 (1992).
[6] Y. Uno, Y. Uwamino, T. S. Soewarsono, and T. Nakamura, Nucl. Sci. Eng. **122**, 27 (1996).
[7] P. J. Dimbylow, Phys. Med. Biol. **25**, 637 (1980).
[8] S. Padalino, C. Freeman, K. Fletcher, E. Pogozelski, J. McLean, and M. Yuly, "Nuclear and Plasma Diagnostics for4 the EP-OMEGA Laser Systems and the NIF," 2013.
[9] V.G.J. Stoks, R.A.M. Klomp, M.C.M. Rentmeester, and J.J. de Swart, Phys. Rev. C **48** 792-815 (1993); V.G.J. Stoks, R.A.M. Klomp, C.P.F. Terheggen and J.J. de Swart, Phys. Rev. C **49** 2950-2962 (1994).
[10] M. Drosg, IAEA report IAEA-NDS-87 Rev. 5 (2000).
[11] S. Padalino, C. Freeman, K. Fletcher, E. Pogozelski, J. McLean, and M. Yuly, "Nuclear and Plasma Diagnostics for4 the EP-OMEGA Laser Systems and the NIF," 2014.
[12] S. Agostinellia, et al., NIM A **506** 250-303 (2003); J. Allison, et al., IEEE Trans. on Nucl. Sci. **53** 270-278 (2006).
[13] E. Schönfeld, U. Schötzig, E. Günther and H. Schrader, Appl. Radiat. Isot. **9**, 955 (1994).
[14] J. Streets and D. Slimmer, Fermilab Report PN540 v. 1.9.2, 2002.

[15] Rene Brun and Fons Rademakers, ROOT - An Object Oriented Data Analysis Framework, Proceedings AIHENP'96 Workshop, Lausanne, Sep. 1996; Nucl. Inst. & Meth. in Phys. Res. A 389 81-86 (1997). See also http://root.cern.ch/.